

A numerical method for the determination of flow-induced damping in hydroelectric turbines

J.P. Gauthier^{a,b,*}, A.M. Giroux^b, S. Etienne^a, F.P. Gosselin^a

^a*Department of Mechanical Engineering, Ecole Polytechnique, Montreal, QC, Canada*

^b*IREQ — Hydro-Quebec Research Institute, Varennes, QC, Canada*

Abstract

To estimate structural fatigue, vibrational response to realistic spectrum of excitations and associated equivalent damping are of paramount importance. In this paper, an approach to quantify flow-induced damping of a relatively heavy fluid on a vibrating hydraulic turbine blade using numerical simulations is presented. First, mode shapes and frequencies of the immersed structure are obtained by modal analysis using the finite element method. Then, forced oscillatory modal motion is prescribed on the structural boundary of unsteady Reynolds-averaged Navier-Stokes flow simulations. Damping is finally computed as the normalized work done by the resulting fluid load on the structure. Validation is achieved by comparing the numerical results with available experimental data for a steel hydrofoil oscillating in flowing water. For this case, the linear increase in the damping ratio with the flow velocity is reproduced within 10% of the experimental values. Application of the method to an actual hydroelectric propeller turbine blade yields a fluid damping value of around 15% of critical damping for its first vibration mode.

Keywords: Added damping, Hydroelectric turbine, Vibration, CFD

1. Introduction

Modern hydroelectric turbines are designed to achieve near perfect efficiency while keeping production costs as low as possible. One way to accomplish such a goal is by reducing the thickness of turbine blades, consequently lowering their stiffness and increasing their propensity to experience critical vibration levels. Moreover, the end-users' growing need for power regulation due to the integration of intermittent renewable sources leads to more frequent off-design operations as well as machine starts and stops, for which dynamic mechanical stresses are significantly higher than at best efficiency point. In this context, precise knowledge of the turbine dynamic characteristics, especially damping, is essential in order to correctly estimate their fatigue life.

The primary function of water flow through a hydroelectric turbine is to impart rotational motion to the runner, but it affects the structure in multiple other ways. For example, the passage of turbine blades in front of guide vanes induces high frequency water pressure variations, which in turn could excite a vibration mode of the runner. This

*Corresponding author.

Email address: jean-philippe.gauthier@polymtl.ca (J.P. Gauthier)

phenomenon, known as rotor-stator interaction (RSI), has been linked to very early cracking of Francis turbine blades [1]. This particular ability of the flow to act as an excitation force has received much attention in recent years and can now be predicted using computational fluid dynamics (CFD) with sufficient precision for design purposes [2, 3]. Many other phenomena can negatively affect the lifetime of a turbine; a review of fatigue mechanisms was recently published by Liu et al. [4].

Hydroelectric turbines are also susceptible to strong fluid-structure interactions (FSI) because of the high density of water relative to that of the runner material, generally steel. It is common to model FSI effects as fluid-added mass, damping and stiffness implemented in the structural equations of motion [5, 6]. For a hydraulic turbine, added mass and added stiffness effects are well understood and relatively easy to model [7]. However, while added damping effects have been investigated for fluid conveying pipes, cables, bridges, cylinder arrays in heat exchangers [5, 6, 8] and also aerodynamic fan blades [9], little research effort has been devoted to water flow-induced damping in hydraulic turbines. Recent work has focused on the experimental determination of damping on simplified hydrofoil geometries [10, 11, 12], along with the development of analytical and numerical models able to reproduce and predict those results [13, 14]. Yet, to the authors' knowledge, these models have not been applied to a real turbine geometry.

Different approaches were considered in order to reproduce the experimental data and predict fluid damping on hydrofoils. Liaghat et al. [14] carried out two-way FSI simulations and related damping to the exponential decay rate of the immersed structure's response to an impulse. A slight dispersion of the numerical results both below and above experimental data was observed, but a good agreement with an average overestimation of 12% was found. Monette et al. [13] proposed a theoretical model based on kinetic energy transfer between the fluid flow and the moving structure. The implementation of this model in an in-house FE code yielded an excellent agreement with experiments, which was also observed when they used prescribed-motion CFD as detailed in this paper.

Conceptually, a decay test remains the simplest approach to estimate flow-induced damping. This method however relies on 2-way coupling of the fluid flow and the structural dynamics. For that reason, its implementation can become cumbersome, particularly for complex industrial machines such as hydroelectric turbines. The method proposed in this paper is based on prescribed motion of the structural boundary in URANS simulations. Consequently, 2-way coupling is not required, but the natural frequency of the coupled system must be known beforehand. Prior modal analysis and steady RANS simulations are used to determine the structural as well as the fluid-added mass and stiffness, from which the natural frequency can be derived. This method remains relatively easy to use in complex geometries. Furthermore, it breaks down the problem of estimating fluid damping into parts, leading to an added understanding of the involved physics.

The main contribution of this work is the prediction of water flow-added damping on an actual hydroelectric propeller turbine blade using numerical simulations. Assuming that FSI do not affect linear independence and orthogonality between the runner's eigenmodes, fluid-added damping is computed for one mode at a time. The following modeling sequence to achieve this is proposed:

1. obtain the mode shape and added mass using modal analysis;
2. obtain added stiffness using steady-state CFD;
3. compute the system's undamped natural frequency taking into account added mass and added stiffness;
4. compute the damping ratio as the normalized work done by the flow on the structure being subjected to prescribed modal oscillations using unsteady CFD.

This paper first introduces the physical vibration model considered. The added damping calculation method is then described. Subsequently, results for a simple hydrofoil which was previously studied experimentally [11, 12] are presented to assess the method. Finally, results for a real propeller turbine blade are given and discussed. This specific power unit in the Canadian province of Quebec was selected because it was recently instrumented for a measurement campaign.

2. Physical model

Assuming independent and orthogonal eigenmodes, the dynamic response of a structure can be described using mode superposition. Furthermore, if only one mode is contributing, the entire structure can be modeled as a single degree of freedom (DOF) linear oscillator. Arguing that structural damping can be neglected as it is much lower than fluid damping [11], the equation of motion for this system is

$$M_S \ddot{h} + K_S h = F_F(t), \quad (1)$$

where M_S is the structural modal mass, K_S the structural modal stiffness, $F_F(t)$ the total modal force applied on the structure by the fluid and h the modal deflection of the structure. The overdot denotes time differentiation. Introducing the shape of the selected mode, $\varphi(x, y, z)$, the structural modal mass and the total modal force can be expressed as follows:

$$M_S = \iiint_{\Omega} \rho_S \varphi^2 dV, \quad (2)$$

$$F_F(t) = \iint_{\Gamma} \tau(t) \cdot \varphi dS, \quad (3)$$

where ρ_S is the density of the structure, Ω the volume of the structure, τ the total surface load induced on the structure by the flow and Γ the fluid-structure interface.

Assuming that fluid-added mass, damping and stiffness depend linearly on acceleration, velocity and displacement, Eq. (1) can be rewritten as

$$(M_S + M_F) \ddot{h} + C_F \dot{h} + (K_S + K_F) h = \tilde{F}_F(t), \quad (4)$$

where M_F is the fluid-added modal mass, C_F is the fluid-added modal damping coefficient, K_F is the fluid-added modal stiffness and $\tilde{F}_F(t)$ is the remaining part of the total fluid force, $F_F(t)$, i.e.

$$F_F(t) = \tilde{F}_F(t) - M_F \ddot{h} - C_F \dot{h} - K_F h. \quad (5)$$

The added mass can be interpreted as the mass of fluid accelerated due to the motion of the structure. The added stiffness describes the change in the flow-induced restoring force with the deflection of the structure. For example, the lift coefficient versus the angle of attack slope for a thin airfoil would correspond to a negative K_F value. The added damping represents energy extracted from the structure as a result of work done by the fluid flow. The remaining force term, $\tilde{F}_F(t)$, may be interpreted as an external excitation, such as forces due to RSI in the case of a turbine.

Taking into account structural mass and stiffness as well as fluid-added effects, the undamped natural frequency of the system is

$$\omega_n^2 = \frac{K_S + K_F}{M_S + M_F}, \quad (6)$$

and the dimensionless ratio of the fluid-added damping coefficient to the critical damping coefficient is given by

$$\zeta = \frac{C_F}{2\omega_n(M_S + M_F)}. \quad (7)$$

3. Method

Every parameter needed to compute the fluid-added damping ratio from Eq. (7) can be obtained using standard numerical methods. The following section describes the three types of simulation required: modal analysis, steady-state CFD and unsteady CFD.

3.1. Modal analysis

In order to compute natural frequencies and mode shapes of a structure immersed in a fluid at rest, fluid-added mass effects can be taken into account using the finite element (FE) method. To achieve this, structural elastic elements are coupled with potential flow elements [15, 16]. Some FE codes have potential flow elements based on the Laplace equation, whereas others have acoustic elements based on the Helmholtz equation. Both types are suitable as the Laplace equation is the degenerate form of the Helmholtz equation for an incompressible fluid, which is a valid assumption for water. Using this method, simulation results on a Francis turbine reduced-scale model immersed in water showed a very good agreement with measured natural frequencies [17, 7]. Of course, the fluid in a running hydroelectric turbine is not at rest but the flow velocity does not seem to influence added mass effects for the problems addressed in this paper. Still, a way to assess the added mass obtained from modal analysis using unsteady CFD results is introduced in section 3.3.

An initial classical modal analysis, *i.e.* modeling only the structure will yield its natural frequency in vacuum, ω_v , which depends only on structural parameters:

$$\omega_v^2 = \frac{K_S}{M_S}. \quad (8)$$

A second structural-potential flow modal analysis will yield the natural frequency of the structure in fluid at rest, ω_{fr} . The only fluid effect taken into account is the added mass:

$$\omega_{fr}^2 = \frac{K_S}{M_S + M_F}. \quad (9)$$

Because a potential flow modeling approach is used, the added mass due to viscous effects is not taken into account. However, for low angles of attack, the wake behind a streamlined body is thin and viscous effects remain weak. Therefore, this approximation is acceptable for hydrofoils and turbine blades. The second modal analysis will also give the mode shape of the structure in still fluid, φ , which is expected to be only slightly different from that in vacuum. For this purpose, both are considered equal, although further calculations will be made using the mode shape of the immersed structure. Additionally, it is assumed that the mode shape is not affected by the additional stiffness induced by the flow.

Using the discrete representation of φ at the nodes of the FE model, the structural modal mass, M_S , can be computed by numerically integrating Eq. (2). The structural modal stiffness, K_S , and the fluid-added modal mass, M_F , are then obtained from Eqs. (8) and (9).

3.2. Steady-state CFD

Assuming the existence of a steady-state flow solution around a motionless structure, the fluid force model (Eq. 5) can be rewritten as the sum of two time-independent forces, one is a constant while the other is proportional to the modal deflection:

$$F_F = F_0 - K_F h. \quad (10)$$

The fluid-added modal stiffness, K_F , corresponds to $-\frac{dF_F}{dh}$. Therefore, RANS flow simulations for at least two different values of h are required in order to quantify K_F . In Eq. (10), it is assumed that the deflection remains small so that the linear approximation holds.

Interpolation of the mode shape onto the CFD mesh must be done in the likely case of non-matching meshes at the fluid-structure interface. To achieve this, it was found that using regression polynomials to obtain a continuous analytical representation of the discrete mode shape was a robust and simple way to implement the method. However, this may not be feasible when working with very complex mode shapes and geometries, in which case direct interpolation of displacement values on the fluid mesh nodes might be a better solution. Modern CFD software often includes mesh deformation algorithms that can easily and automatically manage mesh deformation.

3.3. Unsteady CFD

Knowing the fluid-added modal stiffness, the natural frequency of the fluid-structure coupled system, ω_n , can be computed from Eq. (6). Then, for a prescribed harmonic modal motion of the structure defined by

$$h(t) = h_0 \sin(\omega_n t), \quad (11)$$

a URANS simulation of the surrounding fluid flow can be carried out. An averaged quantity, Φ , is introduced by projecting the resulting modal force time signal, $F_F(t)$, on the prescribed modal deflection, $h(t)$:

$$\Phi = \frac{1}{N} \int_{t_0}^{t_0 + 2\pi N / \omega_n} F_F \cdot h \, dt, \quad (12)$$

In the above expression, N is an integer number of oscillations and t_0 an arbitrary time coordinate. The physical meaning of Φ is not relevant, but it can easily be evaluated by numerically integrating the unsteady CFD results. Assuming that the frequency spectrum of $\tilde{F}_F(t)$ does not contain the system's natural frequency and using a sufficiently high number of periods, substitution of Eq. (5) into Eq. (12) yields the following approximation:

$$\Phi = \frac{\pi h_0^2}{\omega_n} (\omega_n^2 M_F - K_F). \quad (13)$$

Considering that the value of K_F obtained from steady-state CFD results is valid, a new M_F value can be extracted from Eq. (13). An updated natural frequency can be computed from this new added mass and used in a subsequent unsteady CFD simulation. This approach can be implemented iteratively to validate or adjust added mass values obtained from modal analysis.

Similarly, the average modal work done by the flow on the structure, W , can be obtained if the modal force is projected on the modal velocity, \dot{h} , instead of the modal displacement:

$$W = \frac{1}{N} \int_{t_0}^{t_0+2\pi N/\omega_n} F_F \cdot \dot{h} \, dt. \quad (14)$$

Again considering that $\tilde{F}_F(t)$ has negligible contribution at frequency ω_n , for a large enough number of cycles, the expression of modal work can be reduced to the following approximation:

$$W = -C_F \pi h_0^2 \omega_n. \quad (15)$$

This shows that the net work associated with any forcing frequency different from the system's natural frequency will vanish over time. Furthermore, no net work is done by added mass and stiffness effects, as they are conservative forces. The fluid-added modal damping coefficient, C_F , can be obtained by comparing the average modal work computed from CFD results (Eq. 14) to the right-hand side of Eq. (15). The dimensionless fluid-added damping ratio, ζ , can ultimately be determined from Eq. (7).

4. Results

Fluid-added damping was first determined for a steel hydrofoil vibrating in flowing water, for which good agreement between numerical results and experimental data was found. The method was then applied to a real hydroelectric propeller turbine operating at full load. The results are presented and discussed below.

4.1. Hydrofoil

The geometry of the hydrofoil used for validation is schematized in Fig. 1. The channel in which water flows has the same height as the mounting blocks. This test case was introduced by Seeley et al. [11] and Coutu et al. [12], who measured the damping characteristics experimentally. During preliminary testing, they determined that the structural damping ratio was approximately 0.2% and thus structural damping could be neglected. The exact dimensions of

the hydrofoil cannot be divulged as they are protected by a non-disclosure agreement. For various flow velocities, piezoelectric actuators were used to excite the first eigenmode of the immersed structure. Assuming zero structural damping, fluid-added damping was determined from the amplitude of the resulting vibrations, which was measured using a laser vibrometer.

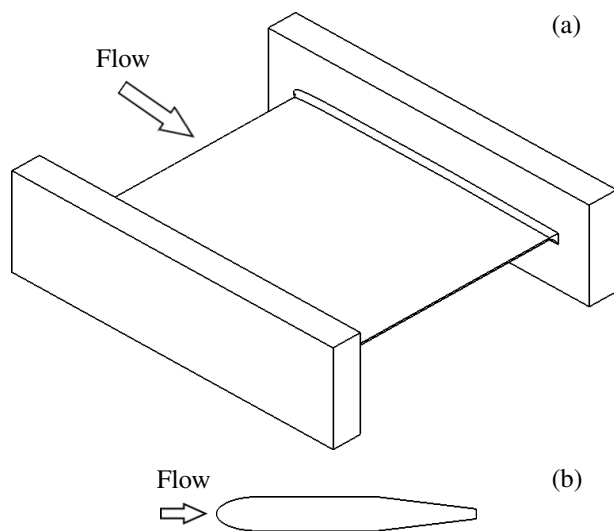


Figure 1: Geometric model of the hydrofoil: (a) isometric view; (b) section of the blade. Not to scale: dimensions were altered to protect intellectual property.

Before discussing these results, it is important to explain why this particular test case, while geometrically very simple, is a pertinent first step towards the evaluation of fluid damping on a real turbine blade. The most obvious point is the use of the same materials, water and steel, so that both problems exhibit the same fluid to structure density ratio and therefore the same modeling challenges associated with added mass effects. Most importantly, this test case was designed so that its characteristic solid timescale T_S (inverse of natural frequency) and fluid timescale T_F (average time taken by a fluid particle to flow around the structure) were close to each other. This is also the case for the first modes of turbine blades, as will be shown in section 4.2. One can instinctively understand that interactions at the fluid-structure interface are the strongest for similar timescales, when energy and momentum exchanges are maximized. This strong coupling is generally expressed as:

$$U_R = \frac{T_S}{T_F} \approx 1, \quad (16)$$

where U_R is known as the dimensionless reduced velocity [6, 18]. A strong fluid-structure coupling is the main reason why quasistatic and pseudostatic approaches are not applicable here, requiring the use of transient CFD. These important fluid-structure considerations as well as the slender turbine blade-like geometry of the hydrofoil demonstrate the pertinence of the test case.

Modal analysis of the hydrofoil was conducted using ANSYS Workbench 15.0 augmented with an extension facilitating the coupling of structural and potential flow elements based on the Helmholtz equation. A single unstructured mesh was generated for both the hydrofoil and the water channel, *i.e.* with shared nodes at the fluid-structure interface. Null-displacement boundary conditions were prescribed on the external faces of both mounting blocks. Solid wall conditions were applied to every boundary of the water channel, including the two that would in reality correspond to the inlet and the outlet. In order to eliminate pressure reflection effects on these two boundaries, the flow-wise length of the modeled channel was iteratively increased until convergence of the computed frequencies. Likewise, the initial FE mesh was refined until convergence was reached.

Results are shown in Table 1. The frequencies computed for the first mode compare well with the numerical predictions made by Seeley et al. [11] and Coutu et al. [12], which are close to their experimental observations. It is interesting to point out that these authors also observed a fairly constant natural frequency in flowing water over a relatively wide range of flow velocities. This observation led Monette et al. [13] to believe that added stiffness, albeit dependent on flow velocity, might remain small for the hydrofoil case. Results that are in agreement with this conclusion are presented later in this paper. The dependence on flow velocity is easily understood when recalling the airfoil lift coefficient example for added stiffness [18].

Table 1: Numerical predictions of natural frequencies and modal parameters for the first mode of the hydrofoil.

	f_v (Hz)	f_{fr} (Hz)	M_F/M_S	K_S (kN/m)
Present work	221	72.7	8.23	396
Seeley et al. [11], Coutu et al. [12]	226	74.9	–	–

The shape of the mode obtained by modal analysis is illustrated in Fig. 2. Statically prescribing this deflection on the hydrofoil, steady RANS calculations of the flow were carried out in ANSYS CFX 15.0. The standard $k - \epsilon$ turbulence model was used along with scalable wall functions. Water velocities U of 1 m/s, 4 m/s, 8 m/s, 12 m/s and 16 m/s were considered in order to cover the range of available experimental results. For each velocity, simulations were conducted for multiple modal deflections ranging from 0 mm to 0.05 mm, the order of magnitude observed in the experiments. Integration of the total modal force (Eq. 3) was done using CFX post-processing tools and plotted in Fig. 3 for each point simulated in the flow velocity/modal deflection parameter space. Calculations were done on a structured mesh comprising around 200 k hexahedral cells.

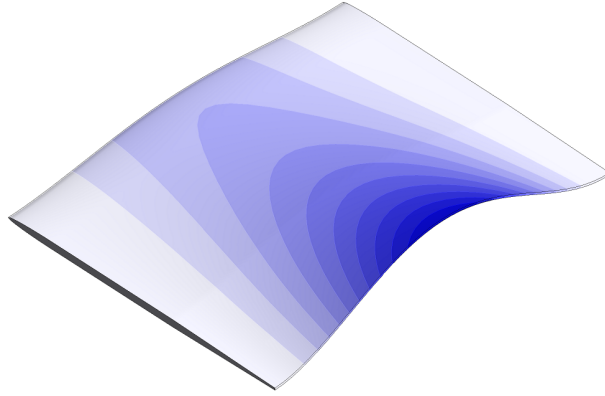


Figure 2: Total displacement field for the first mode of the hydrofoil. Darker coloration represents higher displacement amplitudes; color intensity is linear with respect to displacement.

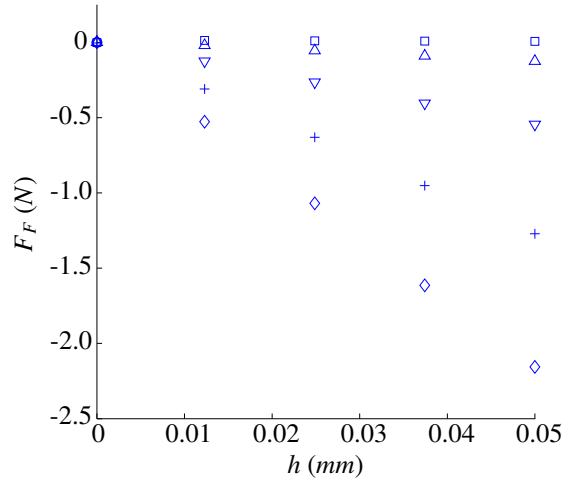


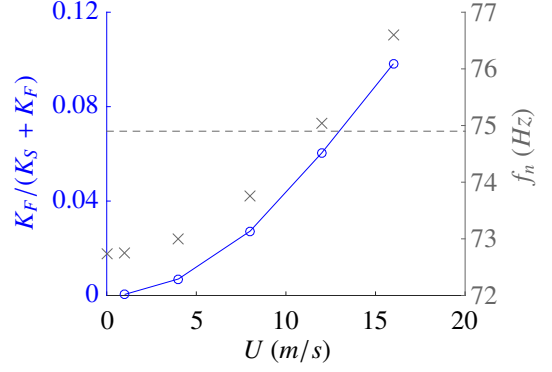
Figure 3: Effect of static modal deflection on the steady modal force induced on the hydrofoil for various flow velocities: 1 m/s (□); 4 m/s (△); 8 m/s (▽); 12 m/s (+); 16 m/s (◇). The linear behavior is consistent with the assumption of a constant fluid-added stiffness.

The modal force exhibits linear dependency on the modal deflection, h , an expected behavior since the prescribed displacements are small. For all flow velocities considered in the simulations, the force is very close to zero when the structure is undeformed. This is due to the symmetry of the problem and the shape of the mode. When no deflection is prescribed, the local surface load τ on the structure is essentially shear stress in the direction of the flow, while the mode shape deflection vector φ is mostly normal to the flow, thus the scalar product in Eq. (3) is almost null. Added stiffness is evaluated by fitting results to the linear model of Eq. (10) using the least squares regression method. Natural frequencies of the flow-structure system are presented in Table 2 and Fig. 4 along with values of K_F .

Table 2: Added stiffness and natural frequency of the first mode of the hydrofoil in flowing water for various flow velocities.

U (m/s)	K_F (kN/m)	f_n (Hz)
0 (modal analysis)	–	72.7
1	0.176	72.8
4	2.79	73.0
8	11.1	73.8
12	25.5	75.0
16	43.2	76.6

Figure 4: Effect of flow velocity on added stiffness and natural frequency: ratio of added to total stiffness (\circ); f_n , numerical (\times); f_n , experiments [11, 12] (---).



An expected quadratic increase in added stiffness with flow velocity is observed. However, for the velocities considered, there is little change in the natural frequency. In fact, the above frequency range is well within that experimentally observed by Seeley et al. [11] and Coutu et al. [12] for this geometry. These authors could not detect a clear trend between natural frequency and flow velocity. They indicated that error on their measurements increased with flow velocity due to noise in their data. This led them to consider a constant natural frequency of 74.9 Hz for every tested flow velocity. For $U = 16$ m/s, where the effect is the strongest, modal added stiffness still only accounts for around 11% of modal structural stiffness. By contrast, the modal added mass is more than *eight* times higher than the modal structural mass, as shown in Table 1. Nonetheless, while added stiffness is less important than added mass, it cannot always be neglected. For example, it leads to a 5% increase of the natural frequency of the hydrofoil when the flow velocity is 16m/s.

Unsteady RANS calculations of the flow with prescribed harmonic modal deflection of the hydrofoil as defined in Eq. (11) were carried out in CFX. A different natural frequency was prescribed for each simulated velocity, as listed in Table 2. For every case, the same vibration amplitude, $h_0 = 0.05$ mm, was used and 10 periods of oscillation were simulated for a 200 k cells mesh for three different time step values corresponding to 200, 400 and 800 time steps per period. A backward Euler second-order time integration scheme was used. A typical sample of the time evolution of the flow-induced modal force, $F_F(t)$, is plotted in Fig. 5.

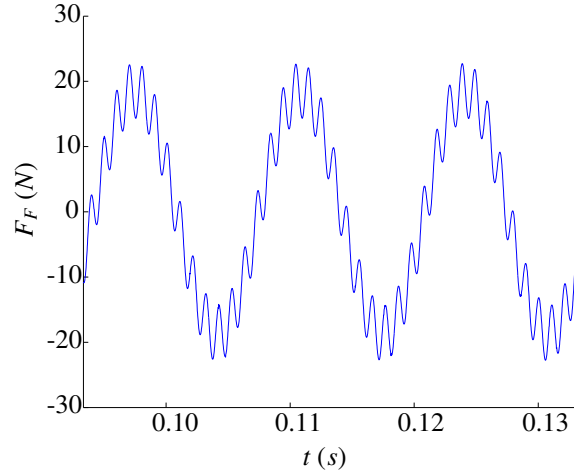


Figure 5: Time evolution of the modal force induced on the oscillating hydrofoil for $U = 12$ m/s. Only the three last simulated periods are shown.

In addition to the primary harmonic component of the force attributed to the prescribed motion, a phenomenon of higher frequency and lower amplitude is clearly visible on the plot. It was observed that this secondary frequency increased with the water velocity following an almost linear trend. It was suspected that this secondary frequency was due to trailing edge vortex shedding characterized by the Strouhal number defined as:

$$St = \frac{f_s b}{U}, \quad (17)$$

where f_s is the vortex shedding frequency and b the thickness of the trailing edge of the body. This hypothesis was confirmed using three-dimensional visualization of the flow solution. For $U = 1$ m/s, no secondary frequency was observed in the force signal. This indicates that lock-in might be occurring between the shedding frequency and the hydrofoil's natural frequency [19]. To verify this, additional URANS simulations were conducted to determine the Strouhal numbers associated with vortex shedding in the wake of a static hydrofoil. Results for these vortex shedding frequencies are plotted against flow velocity in Fig. 6 and exhibit a Strouhal number around $St \approx 0.15$. The natural frequency of the hydrofoil is also shown. It can be seen that the intersection of both data sets happens when the flow velocity is very close to $U = 1$ m/s. This evidence suggests the occurrence of frequency lock-in at this flow velocity.

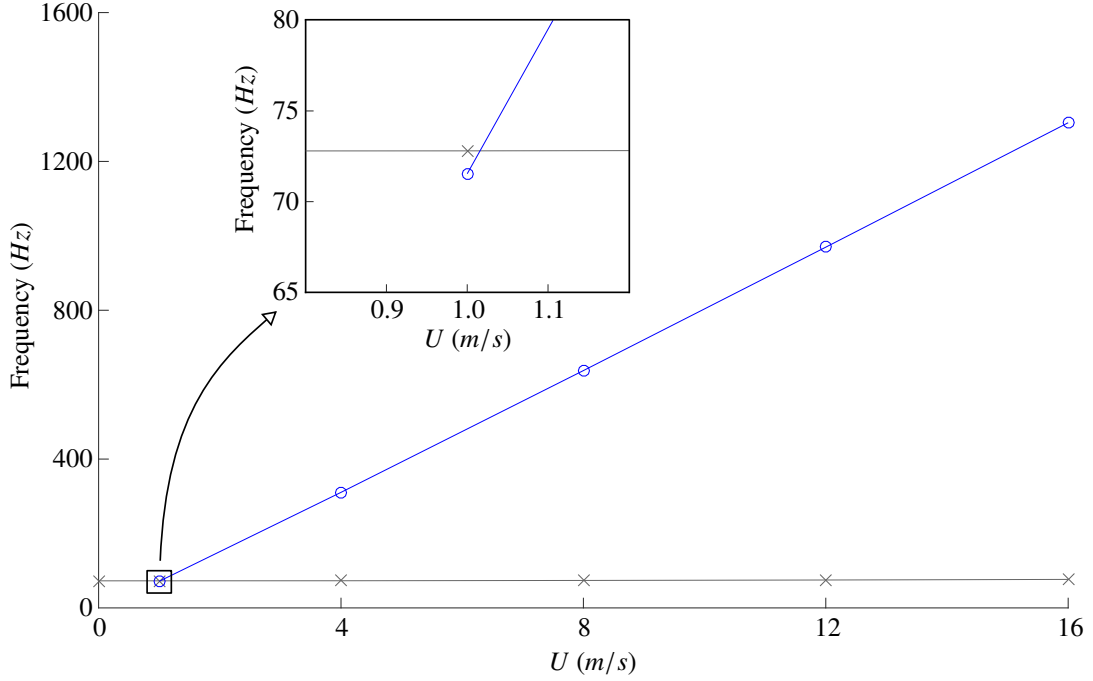


Figure 6: Frequency lock-in seems to appear near $U = 1$ m/s. Vortex shedding frequency of the fixed hydrofoil (Strouhal number, $St \approx 0.15$) (\circ); natural frequency of the hydrofoil (\times).

Validation of added mass was achieved by comparison with CFD results. For every flow velocity, no significant differences were observed between the values of M_F obtained from modal analysis and those obtained from Eqs. (12) and (13). CFD values remain within 2% of modal analysis results, as shown in Table 3. This supports the assumption that added mass is independent from flow velocity for the hydrofoil.

Table 3: Variation of added mass obtained using CFD relatively to modal analysis results.

U (m/s)	$(M_{F,CFD} - M_F)/M_F$
1	-1.1 %
4	-1.7 %
8	-2.0 %
12	-1.5 %
16	-1.0 %

In Fig. 7, the dimensionless fluid-added damping ratio ζ is plotted against the size of the $F_F(t)$ sample used for its calculation, expressed as a number of oscillation periods, N . In order to show all data on the same plot, ζ is normalized with ζ_{ref} , a reference value different for each simulated velocity which corresponds to ζ computed from the entire 10

periods signal. The first period is discarded in all cases to exclude transients. Four periods are sufficient to reach convergence within 1% of ζ_{ref} , except for $U = 1$ m/s. The relative slow convergence for that case is probably due to the vortex shedding frequency being close to that of the structural motion. As stated in section 3.3, the average net work done on a 1-DOF system oscillating at its natural frequency f_n by a cyclic force of frequency $f \neq f_n$ will eventually vanish over time. However, it can also be demonstrated that the closer the forcing frequency is to the system's frequency, the longer this decay will take as the interaction between forcing and response is stronger.

The influence of the numerical time step size on the computed damping ratio value was found to be of the first order. Results for the coarsest time step size as well as least squares linear extrapolations for an infinitely small step size are plotted against the flow velocity in Fig. 8. Experimental damping values from the experiments of Seeley et al. [11] and Coutu et al. [12] are also shown for comparison. Except for $U = 1$ m/s, neglecting the structural damping ratio of 0.2 % remains a valid assumption as fluid damping is much higher. For $U = 4$ m/s, calculations were also performed on coarsened (down to 25 k cells) and refined (up to 1.6 M cells) meshes. Relatively to the initial mesh, the coarse mesh resulted in a 12% increase in the damping ratio. The refined mesh yielded a 3.4% decrease, which is not that much considering a mesh eight times more dense. The initial mesh is thus regarded as satisfactory. Numerical results compare well with experiments, showing 10% overestimation on the $d\zeta/dU$ value obtained by least squares linear regression for both data sets. This overestimation is mostly contained within the experimental error bars.

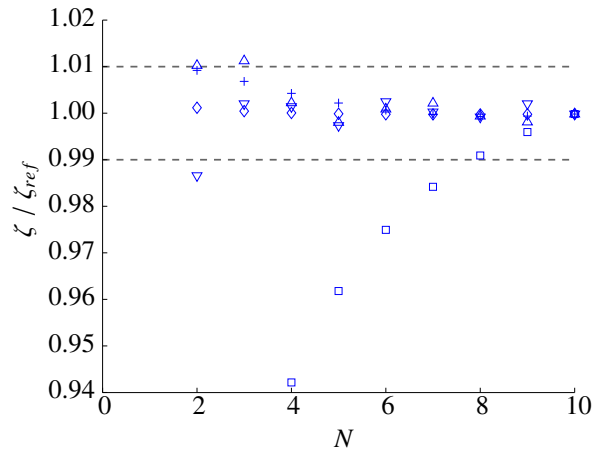


Figure 7: Effect of the number of simulated oscillations on the damping ratio for the hydrofoil for various flow velocities: 1 m/s (□); 4 m/s (△); 8 m/s (▽); 12 m/s (+); 16 m/s (◇). The reference, ζ_{ref} , is obtained from the entire signal (ten periods) for each flow velocity.

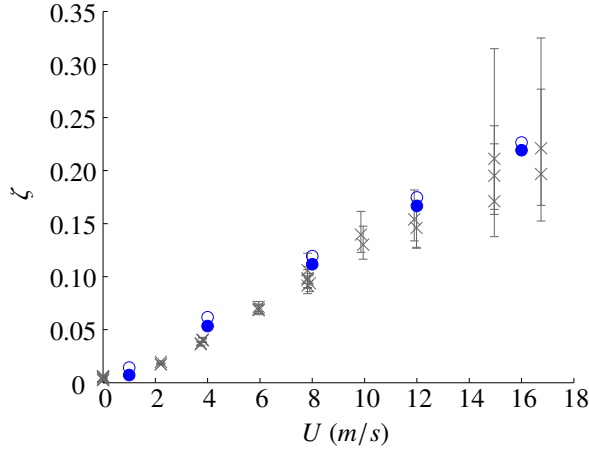


Figure 8: Fluid-added damping ratio for the hydrofoil at various flow velocities: 200 time steps per oscillation (○); linear extrapolations for an infinitely small time step size (●); experiments [11, 12] (×).

To explain the linear increase in damping with flow velocity, the modal motion of the hydrofoil can roughly be approximated by the transverse vibration of a rigid two-dimensional wing, described by the displacement $y(t)$. At first order, the angle of attack, *i.e.* the angle between the wing and the mean flow, is given by $-y/U$. The lift force, being proportional to both the angle of attack and the square of the flow velocity, is ultimately proportional to $-U\dot{y}$, which describes a damping mechanism with a linear relationship to flow velocity.

Overall, it is observed that the proposed method is able to predict not only the general trend of damping linearly increasing with flow velocity, but the absolute value of the damping ratio as well. Systematic refinement of the mesh and time step size tends to decrease the error relative to experiments, however not significantly, suggesting that the gap is mostly caused by other factors. Minor disparities in geometry and material properties between the numerical model and the actual setup are practically unavoidable and might account for some of the error. Also, while only the selected mode shape is prescribed in the simulations, it is probable that the piezoelectric actuators used in the experiments slightly excited a few other modes, whose contribution on the structural response might have affected damping effects. Nevertheless, a 1-DOF linear model was able to successfully reproduce experimental results within a 10% error margin for a coupled fluid-structure system similar to a turbine blade. This is sufficiently promising to test the method on an actual hydroelectric turbine.

4.2. Propeller turbine

Investigation of fluid-added damping was conducted on an actual six-blade propeller turbine presently in operation in the Canadian province of Quebec. The choice of this particular unit was primarily motivated by a recent measurement campaign. An extensive database of pressure sensor and strain gauge readings is now available for various operating conditions. However, this raw data is not readily usable to determine the fluid damping associated with a particular vibration mode. Consequently, experimental data was used mostly to identify dominant frequencies

in the turbine blades' response. This was done to help select a vibration mode which was susceptible to be excited and thus for which the determination of fluid-added damping was relevant.

The runner is depicted in Fig. 9, along with the adjacent sections of a typical hydraulic channel. The upstream part, known as the distributor, aligns the flow with the runner blades using stay vanes and guide vanes. The latter can also rotate in order to control the mass flow rate. The unit considered in this paper comprises 24 vanes of each type. The downstream part is a divergent channel called the draft tube whose role is to reduce the velocity and increase the pressure of the flow exiting the runner.

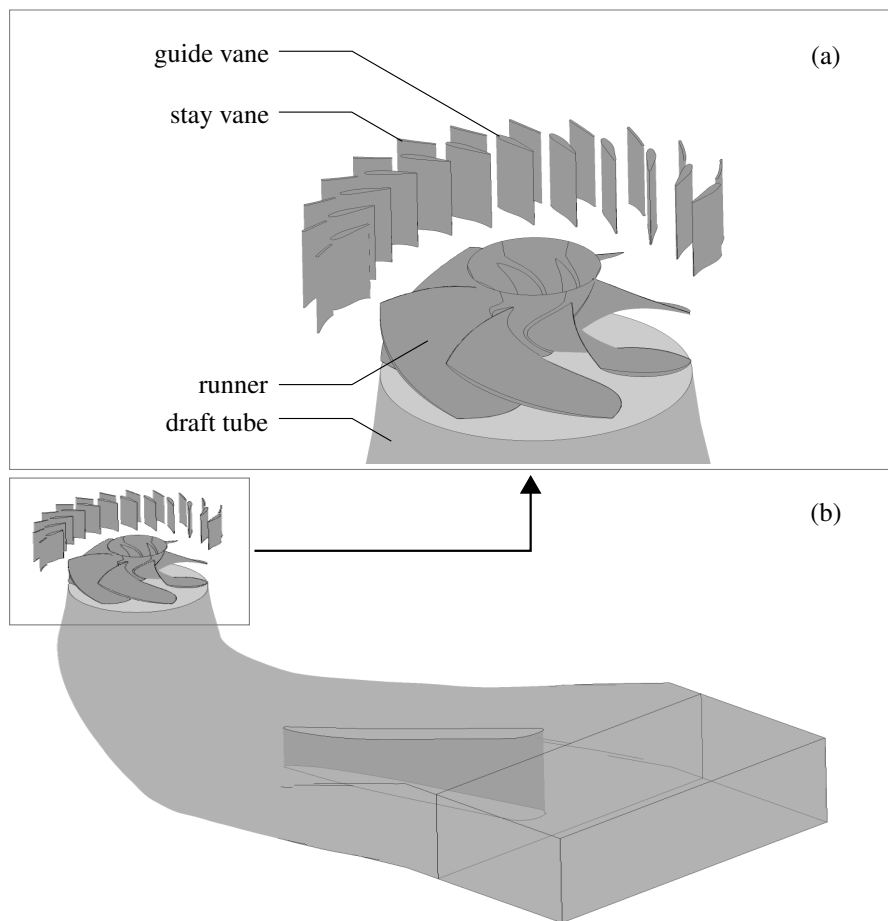


Figure 9: Schematic of the propeller turbine: close-up of the distributor and the runner (a); global view (b). To prevent cluttering the figure, some boundaries were not drawn and only half of the guide vanes and stay vanes are visible. Not to scale: dimensions were altered to protect intellectual property.

Damping was computed only for the turbine operating at full load, or maximum rated power. Under such conditions, the flow in the runner is relatively well aligned with the blades and globally smooth. For the selected turbine, this corresponds approximately to a water mass flow rate of 4×10^5 kg/s and a power of 70 MW. The radius of

the runner, R , and the chord of the blades, c , are both around 3 m. The mean water velocity, U_{mean} , estimated from the mass flow rate and the circular area based on R is of 14 m/s, from which a chord-based Reynolds number of 42 millions can be determined. To simplify the application of the method, it was decided to only consider modes having zero nodal diameter, *i.e.* modes for which the motion of every blade is in-phase. This way, the size of both FE and CFD models can be reduced, in this case by six, using cyclic symmetry boundary conditions. For modes with multiple nodal diameters, the “Fourier Transformation” method [20] could theoretically be used to determine added damping at a lower computational cost than simulating the entire (360°) turbine.

Modal analysis of a single cyclically symmetric blade was done in ANSYS Workbench 15.0. A single unstructured mesh for both the blade and the surrounding water with shared nodes at the interface was built. The shape of the fluid domain was modeled as close as possible to reality using available drawings. However, to increase the stability of meshing algorithms, the radial gap of a few millimeters between the tip of the blade and the casing was suppressed by extending the blade. This slight elongation is not significant compared to the radius of the turbine and does not affect the natural frequencies of the structure in vacuum. However, the thereby neglected pressure in the tip gap can possibly result in erroneous evaluation of added mass effects. Fortunately, it was possible to reassess the added mass using the results of transient CFD, where the blade tip gap was modeled. The modal analysis results were used as a good initial guess.

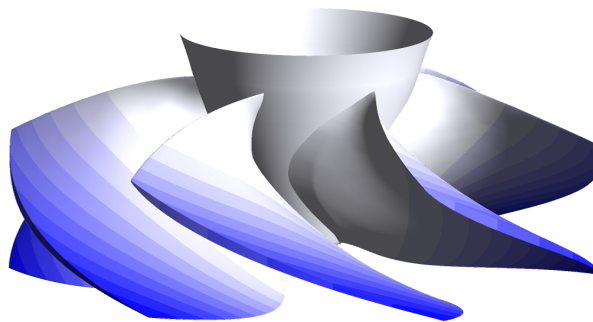


Figure 10: Total displacement field for the first mode with zero nodal diameter of the propeller turbine. Darker coloration represents higher displacement amplitudes; color intensity is linear with respect to displacement.

Refinement of an initial mesh comprising approximately 65 k nodes up to a final mesh of around 500 k nodes showed good convergence of computed frequencies, as shown in Fig. 11. The first mode with zero nodal diameter was retained. Its associated deflection is mostly blade bending, as illustrated in Fig. 10. Relevant frequencies and modal parameters are listed in Table 4.

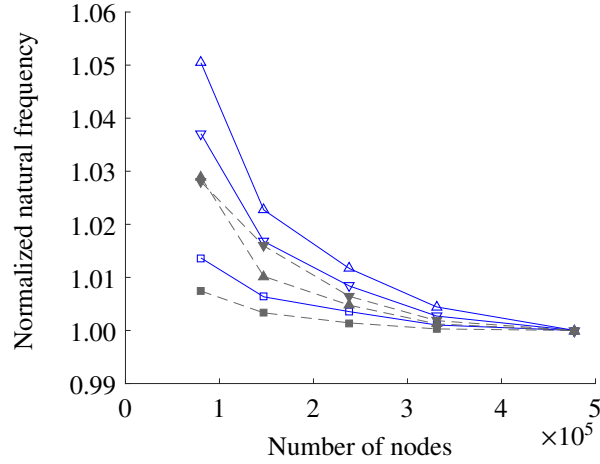


Figure 11: Mesh sensitivity analysis for zero nodal diameter modes of the propeller turbine: 1st mode in water (\square); 2nd mode in water (\triangle); 3rd mode in water (∇); 1st mode in vacuum (\blacksquare); 2nd mode in vacuum (\blacktriangle); 3rd mode in vacuum (\blacktriangledown).

Table 4: Numerical predictions of natural frequencies and modal parameters for the first mode of the propeller turbine.

f_v (Hz)	f_{fr} (Hz)	M_F/M_S	K_S (kN/m)
22.2	10.4	3.59	1.54×10^4

Steady-state CFD simulations were conducted in CFX 15.0 for various modal deflections using the standard $k - \epsilon$ turbulence model and scalable wall functions. Around 830 k, 1.4 M and 1.8 M hexahedral cells were used to mesh the entire draft tube, one sixth of the distributor and one sixth of the runner (one blade) respectively. Circumferential averaging interfaces were used to convey flow variable information between the subdomains. Velocity components corresponding to operation at full load were prescribed at the distributor inlet while an average zero pressure condition was set on the draft tube outlet. Results for the modal force on the blade are plotted against the modal deflection in Fig. 12. The observed linear behavior translates to a constant added modal stiffness, given in Table 5 along with the natural frequency of the turbine in flowing water.

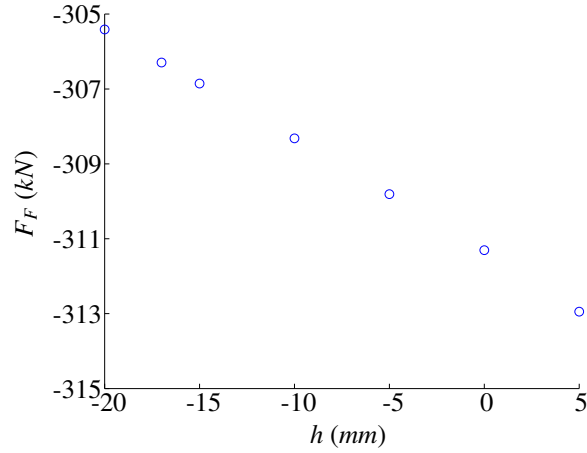


Figure 12: Effect of static modal deflection on the steady modal force induced on the propeller turbine blade when operating at full load. The constant added stiffness is the slope of the linear relation.

Table 5: Effect of fluid-added stiffness on the natural frequency of the turbine's first mode.

Case	K_F (kN/m)	f_n (Hz)
No flow (modal analysis)	–	10.4
Full load	299	10.5

An important remark can be made here. First, the characteristic timescale of the structure can be expressed as the inverse of the turbine's natural frequency, *i.e.* $T_S = 1/f_n$. Also, the fluid timescale corresponds to the time required for a fluid particle to flow from the leading edge to the trailing edge of a blade, *i.e.* $T_F = c/U_{mean}$. Consequently, the reduced velocity for the propeller turbine operating at full load is $U_R \approx 0.44$, revealing a strong fluid-structure coupling.

The CFD pressure field for the non-deformed runner ($h = 0$) was interpolated on a FE mesh to use as a load in a structural static analysis. The resulting static deflection of the blade was found to be almost identical to the selected mode shape, with an amplitude of $h_{stat} = -17$ mm (negative sign due to the arbitrarily chosen convention for the mode shape deflection). To assess the validity of this one-way fluid-structure analysis, it can be pointed out that:

1. the added modal stiffness is low compared to the structural modal stiffness ($K_F/K_S < 2\%$). Flow-induced stiffness therefore has little effect on the structural deflection;
2. the modal force for $h = -17$ mm is only 1.6% higher than for $h = 0$. This suggests that structural deflection does not significantly affect the flow.

Consequently, one-way coupling was deemed sufficient. To compute damping, modal oscillation of the blade was prescribed around this new equilibrium position. For the sake of simplicity, it was decided to take advantage of the

similarity between the static and modal displacement fields, conveniently allowing the prescribed modal deflection to be expressed as:

$$h(t) = h_{stat} + h_0 \sin(\omega_n t). \quad (18)$$

Of course, if the static and modal displacement fields were different, it would be possible to simply superimpose the two displacement fields, as long as deformations remain small.

In order to reduce computational costs for unsteady RANS simulations, the distributor and the draft tube subdomains were dropped. An inlet velocity field and an outlet pressure field were applied as boundary conditions on the remaining turbine subdomain. These fields were extracted from the $h = h_{stat}$ steady-state solution at the distributor-turbine and turbine-draft tube interfaces, respectively.

A first simulation of 20 oscillations with $h_0 = 1$ mm was performed using a time step size corresponding to 100 time steps per oscillation. This case was used to reassess added mass effects using Eqs. (12) and (13). As shown in Table 6, only a few iterations were necessary for the natural frequency to converge to $f_n = 10.8$ Hz. The tabulated value of M_F for iteration 0 corresponds to modal analysis results.

Table 6: Iterative correction of the natural frequency of the turbine’s first mode.

Iteration	f_n (Hz)	M_F (kg)	f_n (Hz)
	prescribed	updated	updated
0	–	2845	–
1	10.5	2707	10.68
2	10.7	2640	10.78
3	10.8	2651	10.76

Using this corrected natural frequency, the flow in the turbine was simulated for additional vibration amplitudes, h_0 , of 0.01 mm, 0.1 mm and 3 mm. This was done to study the sensitivity of fluid-added damping to this parameter, from very small oscillations to potentially catastrophic vibrations.

A sample of the time evolution of the modal force on the blade is plotted in Fig. 13. Two distinct frequencies are observable in each signal: the prescribed natural frequency as well as a slower 2.3 Hz phenomenon. The former corresponds to the combined effects of added mass, damping and stiffness. The latter was linked to leading edge vortices near the runner hub using 3-D visualization of the flow solution. The force amplitude of the natural frequency component was found to be proportional to the prescribed vibration amplitude. On the other hand, the amplitude of the force attributable to vortex shedding showed no significant dependency on the vibration amplitude. Consequently, for low h_0 values, the contribution of vortex shedding relative to the total force becomes higher than added mass, damping and stiffness effects.

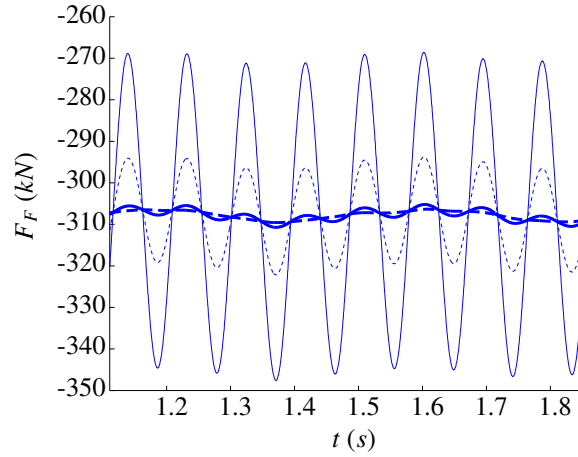


Figure 13: Time evolution of the modal force induced on the oscillating turbine blade at full load for various prescribed vibration amplitudes: 3 mm (—); 1 mm (- - -); 0.1 mm (—); 0.01 mm (- - -). Only the eight last simulated periods are shown.

In Fig.14(a), the fluid-added damping ratio is plotted against the number of oscillation periods used for its calculation. The damping ratio ζ converges to a stable value for the three highest prescribed vibration amplitudes, but not for $h_0 = 0.01$ mm. It is suspected that this convergence problem is due to the amplitude of the motion-induced forces being lower than that of the vortex-induced forces, which can be interpreted as noise when computing the damping ratio. In order to test this hypothesis, the harmonic component of the fluid force, *i.e.* the component whose frequency corresponds exactly to the natural frequency of the system, were extracted from the signal using a fast Fourier transform. Using only this component, a filtered signal was reconstructed and integrated in order to reassess modal work and damping ratio values, which are shown in Fig.14(b). While the convergence is still not fully achieved for $h_0 = 0.01$ mm, the evolution of ζ over simulated time becomes much smoother and high variations from one oscillation period to the next have vanished.

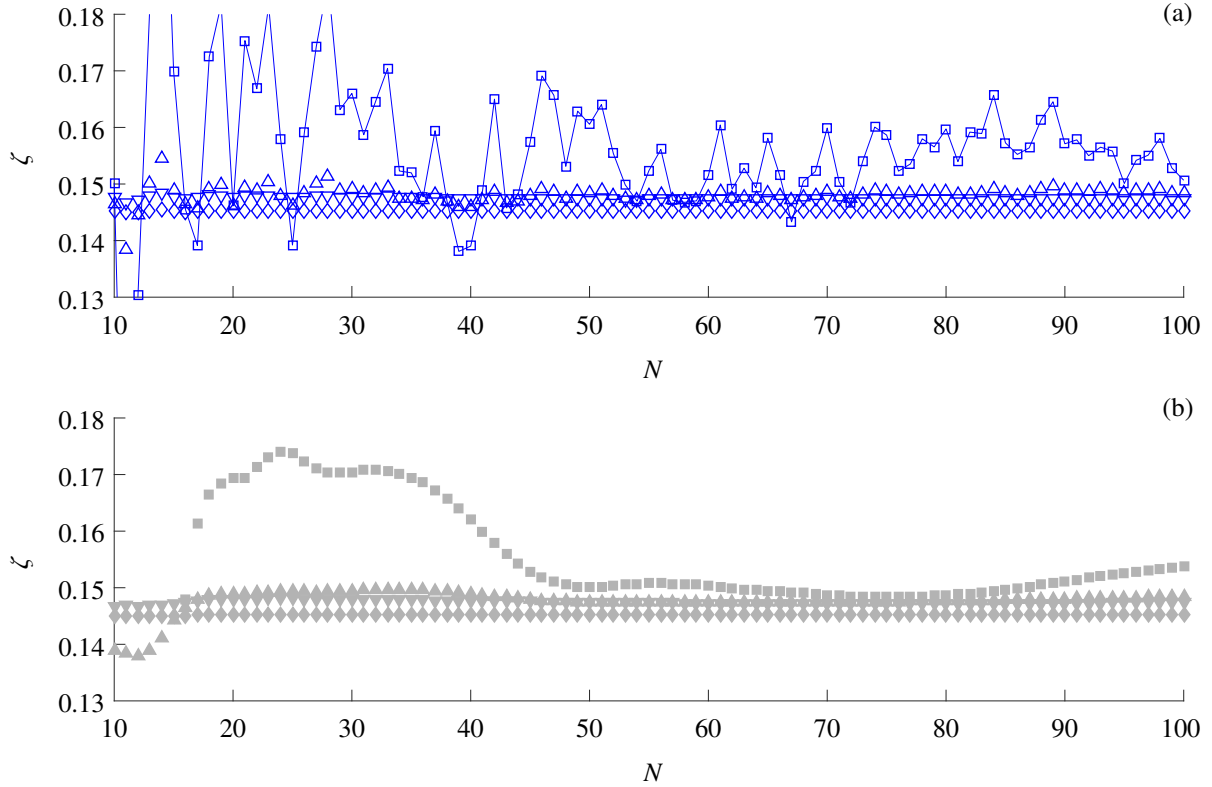


Figure 14: Effect of the number of simulated oscillations on the damping ratio of the turbine blade. In (a), the modal force signal obtained using CFD is integrated directly for various prescribed vibration amplitudes: 0.01 mm (□); 0.1 mm (△); 1 mm (▽); 3 mm (◇). In (b), a reconstructed signal whose frequency content was limited to the natural frequency of the system is integrated: 0.01 mm (■); 0.1 mm (▲); 1 mm (▼); 3 mm (◆).

Furthermore, the overall range of damping ratio values over simulated time is greatly reduced when using this modal decomposition approach. For the last 50 simulated periods, results plotted in Fig.14(b) are comprised inside $\zeta \in [0.145, 0.154]$. This is a relatively small range considering the factor of 300 between the highest and lowest prescribed vibration amplitudes. The sensitivity of the damping ratio to the amplitude of the motion is therefore deemed modest at most. A slight decrease in damping can be observed with increasing vibration amplitude.

5. Conclusion

Damping due to the water flowing around the blades of a hydroelectric turbine can significantly affect its vibrational behavior, which in turn is closely linked to its service life. To characterize this complex fluid-structure interaction problem, an essentially decoupled numerical method, as opposed to a bidirectional fluid-structure coupling, was proposed. Coupling between the fluid and the structure occurs only in the FE model used for modal analysis, where it is relatively easy to implement. Modal motion of the structure is then prescribed in unsteady RANS simulations of the

flow and damping is extracted from the resulting forces. Complementarily, fully coupled fluid-structure simulations could be used to validate the results presented in this paper.

While the proposed approach is interesting for its relatively simple modeling, it is important to understand its main limitations:

- a single vibration mode is considered at a time, neglecting any possible interaction between modes;
- linear modeling of flow-induced forces might not be applicable in more chaotic flows, such as those found in turbines operating at partial load;
- implementation is not trivial and requires time, both human and computational.

The method was validated using a test case consisting of a turbine blade-like hydrofoil oscillating in flowing water. For its first vibration mode, experimental results were numerically reproduced within a 10% margin of error over a range of flow velocities.

When the procedure was applied to the first mode with zero nodal diameter of a hydroelectric propeller turbine operating at full load, an added damping ratio of approximately 15% was determined. Sensitivity to the amplitude of the prescribed modal motion was investigated and found to be low. However, when prescribing small amplitudes, interference with vortex shedding seems to occur, hindering the convergence of the damping ratio over time to a stable value.

Through repeated application of the method for several vibration modes and operating points, a damping *mapping* of a turbine could be established and used to model its dynamic behavior more accurately.

Acknowledgements

Special thanks are due to Andritz Hydro Canada Inc. for greatly facilitating this research by sharing their work on hydrofoils. The authors would also like to thank the Natural Sciences and Engineering Research Council of Canada (NSERC) as well as the Fonds de recherche du Quebec - Nature et technologies (FRQNT) for funding this project.

References

- [1] A. Coutu, D. Proulx, S. Coulson, A. Demers, Dynamic Assessment of Hydraulic Turbines, in: Hydrovision 2004, Montreal, Canada, 2004.
- [2] B. Nennemann, T. C. Vu, M. Farhat, CFD prediction of unsteady wicket gate-runner interaction in Francis turbines: A new standard hydraulic design procedure, in: HYDRO 2005, 2005.
- [3] U. Seidel, B. Hbner, J. Lfflad, P. Faigle, Evaluation of RSI-induced stresses in Francis runners, IOP Conference Series: Earth and Environmental Science 15 (5) (2012) 052010, ISSN 1755-1307, 1755-1315, doi:10.1088/1755-1315/15/5/052010.
- [4] X. Liu, Y. Luo, Z. Wang, A review on fatigue damage mechanism in hydro turbines, Renewable and Sustainable Energy Reviews 54 (2016) 1–14, ISSN 13640321, doi:10.1016/j.rser.2015.09.025.
- [5] M. Paidoussis, Fluid-Structure Interactions: Slender Structures and Axial Flow, Fluid-structure Interactions: Slender Structures and Axial Flow, Elsevier Science, ISBN 978-0-08-053175-5, 1998.

- [6] R. Blevins, *Flow-induced Vibration*, Krieger Publishing Company, ISBN 978-1-57524-183-8, 2001.
- [7] Q. Liang, C. Rodriguez, E. Egusquiza, X. Escaler, M. Farhat, F. Avellan, Numerical simulation of fluid added mass effect on a francis turbine runner, *Computers & Fluids* 36 (6) (2007) 1106–1118, ISSN 00457930, doi:10.1016/j.compfluid.2006.08.007.
- [8] E. Naudascher, D. Rockwell, *Flow-Induced Vibrations: An Engineering Guide*, Dover Civil and Mechanical Engineering, Dover Publications, ISBN 978-0-486-13613-4, 2012.
- [9] P. Vasanthakumar, Computation of aerodynamic damping for flutter analysis of a transonic fan, in: *ASME 2011 Turbo Expo: Turbine Technical Conference and Exposition*, American Society of Mechanical Engineers, 1429–1437, 2011.
- [10] S. Roth, M. Calmon, M. Farhat, C. Mnch, H. Bjoern, F. Avellan, Hydrodynamic damping identification from an impulse response of a vibrating blade, in: *Proceedings of the 3rd IAHR International Meeting of the Workgroup on Cavitation and Dynamic Problems in Hydraulic Machinery and Systems*, vol. 1, Brno University of Technology, 253–260, 2009.
- [11] C. Seeley, A. Coutu, C. Monette, B. Nennemann, H. Marmont, Characterization of hydrofoil damping due to fluidstructure interaction using piezocomposite actuators, *Smart Materials and Structures* 21 (3) (2012) 035027, ISSN 0964-1726, 1361-665X, doi:10.1088/0964-1726/21/3/035027.
- [12] A. Coutu, C. Seeley, C. Monette, B. Nennemann, H. Marmont, Damping measurements in flowing water, *IOP Conference Series: Earth and Environmental Science* 15 (6) (2012) 062060, ISSN 1755-1307, 1755-1315, doi:10.1088/1755-1315/15/6/062060.
- [13] C. Monette, B. Nennemann, C. Seeley, A. Coutu, H. Marmont, Hydro-dynamic damping theory in flowing water, *IOP Conference Series: Earth and Environmental Science* 22 (3) (2014) 032044, ISSN 1755-1307, 1755-1315, doi:10.1088/1755-1315/22/3/032044.
- [14] T. Liaghat, F. Guibault, L. Allenbach, B. Nennemann, Two-Way Fluid-Structure Coupling in Vibration and Damping Analysis of an Oscillating Hydrofoil, in: *ASME 2014 International Mechanical Engineering Congress and Exposition*, American Society of Mechanical Engineers, V04AT04A073–V04AT04A073, 2014.
- [15] O. C. Zienkiewicz, P. Bettess, Fluid-structure dynamic interaction and wave forces. An introduction to numerical treatment, *International Journal for Numerical Methods in Engineering* 13 (1) (1978) 1–16.
- [16] C. Brennen, *A Review of Added Mass and Fluid Inertial Forces.*, Tech. Rep. CR 82.010, Department of the Navy, Port Hueneme, CA, USA, contract Number N62583-81-MR-554, 1982.
- [17] C. Rodriguez, E. Egusquiza, X. Escaler, Q. Liang, F. Avellan, Experimental investigation of added mass effects on a Francis turbine runner in still water, *Journal of Fluids and Structures* 22 (5) (2006) 699–712, ISSN 08899746, doi:10.1016/j.jfluidstructs.2006.04.001.
- [18] E. de Langre, *Fluides et solides*, Editions de l’Ecole Polytechnique, Palaiseau, France, ISBN 978-2-7302-0833-8, 2001.
- [19] E. de Langre, Frequency lock-in is caused by coupled-mode flutter, *Journal of Fluids and Structures* 22 (6-7) (2006) 783–791, ISSN 08899746, doi:10.1016/j.jfluidstructs.2006.04.008.
- [20] S. Connell, M. Braaten, L. Zori, R. Steed, B. Hutchinson, G. Cox, A Comparison of Advanced Numerical Techniques to Model Transient Flow in Turbomachinery Blade Rows, *ASME*, ISBN 978-0-7918-5467-9, 1241–1250, doi:10.1115/GT2011-45820, 2011.